Author's Accepted Manuscript

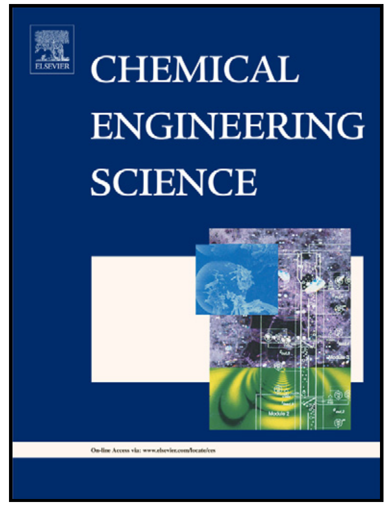

www.elsevier.com/locate/ces

CFD study of droplet atomisation using a binary nozzle in fluidised bed coating

W. Duangkhamchan, F. Ronsse, F. Depypere, K. Dewettinck, J.G. Pieters

PII: S0009-2509(11)00726-3
DOI: doi:10.1016/j.ces.2011.10.022
Reference: CES 10056

To appear in: *Chemical Engineering Science*

Received date: 11 August 2011
Revised date: 6 October 2011
Accepted date: 9 October 2011

Cite this article as: W. Duangkhamchan, F. Ronsse, F. Depypere, K. Dewettinck and J.G. Pieters, CFD study of droplet atomisation using a binary nozzle in fluidised bed coating, *Chemical Engineering Science*, doi:10.1016/j.ces.2011.10.022

CFD study of droplet atomisation using a binary nozzle in fluidised bed coating

Duangkhamchan[a,b], W., Ronsse[a], F., Depypere[b], F., Dewettinck[b], K. & Pieters[a,*], J.G.

[a] *Biosystems Engineering, Faculty of Bioscience Engineering, Ghent University, Coupure links 653, B-9000 Ghent, Belgium*

[b] *Laboratory of Food Technology and Engineering, Faculty of Bioscience Engineering, Ghent University, Coupure links 653, B-9000 Ghent, Belgium*

[*] Corresponding author: Tel.: +32 9 264 61 88; fax: +32 9 264 62 35.

e-mail address: Jan.Pieters@UGent.be

Abstract

An Eulerian-Lagrangian Computational Fluid Dynamics (CFD) model was built to describe two-fluid atomisation in a tapered fluidised bed coater using the air-blast/air-assisted atomiser model. Atomisation was modelled both with and without the inclusion of the solid phase (i.e. gas-liquid and gas-solid-liquid multiphase modelling). In addition, a multi-fluid flow model (Eulerian-Eulerian framework) combined with a population balance model was used as an alternative approach for modelling the spray produced by a two-fluid nozzle. In this approach, the CFD solver couples the population balance equation along with the Navier-Stokes equations for predicting the droplet diameter and mass fraction distribution. Comparison between simulated spray pattern (gas-liquid model) and that experimentally visualised by means of UV illumination was made and a good agreement was obtained. Parametric studies were done in order to investigate the effects of operating conditions on spray cone and liquid mass fraction inside the reactor. Furthermore, comparison of time-averaged fluidised bed

behaviour with the inclusion of sprays obtained by both gas-solid-liquid multiphase modelling methods is presented.

Keywords

Fluidisation, Computational Fluid Dynamics, Multiphase flow, Powder technology, Two-fluid Atomisation, Population balance model

1. Introduction

Among a wide range of microencapsulation techniques, fluidised bed technology has been successfully used for the coating of particulate solids due to its excellent mixing capabilities and its optimal heat and mass transfer rates (Ronsse *et al*., 2007a, b). Fluidised bed coating is an added-value technique whereby a pure active ingredient or mixture of ingredients, in solid particulate form, is encapsulated a within a coating polymer. The aim of encapsulation is to control release, to protect the core ingredients, to increase the overall product quality and to increase the processing convenience. An aqueous or organic solvent-based solution containing the coating polymer is continuously sprayed by means of a pneumatic or two-fluid nozzle, which may be submerged in or positioned above the bed (Depypere *et al*., 2009; Ronsse *et al*., 2007b). In top-spray configuration, regarded as the most appropriate method to be successfully used in the food industry due to its high versatility, relatively high batch size and relative simplicity (Depypere *et al*., 2009), the two-fluid nozzles are usually positioned above the bed, producing sprays of an aqueous solution of the coating material with a droplet size ranging from 10 to 40 µm in order to coat particles (Hede *et al*., 2008; Ronsse *et al*., 2007b).

In top-spray fluidised bed coating, the basic operating principle consists of air suspension of particles in the coating chamber, spraying of coating polymer solution as droplets with the objective of increasing the probability of particle-droplet impact, spreading of droplets on the particle surface, droplet evaporation and layering or superposition of droplets on the particle surface resulting in a homogeneous coating enveloping the core particles (Teunou and Poncelet, 2002). In order to control process efficiency in fluidised bed coating using a model-based approach, it is necessary to explore each phenomenon taking place in the system. As described in previous works (Duangkhamchan *et al*., 2010; Duangkhamchan *et al*., 2011), the momentum transfer between the gas and solid phases was first modelled using various drag coefficient models, in order to evaluate the appropriate drag model for the description of fluidised bed behaviour (Duangkhamchan *et al*., 2010). However, in that work, only interaction between gas and solid phases with the absence of atomisation was taken into account. Subsequently, the solids volume fraction was simulated including the effect of the release of compressed air by the two-fluid nozzle in order to provide qualitative and quantitative consistency of model simulations with experimental data (Duangkhamchan et al., 2011). However, the liquid phase, being the sprayed droplets, was not yet included in the latter study. Therefore, the next step – as outlined in this research article – is the addition of the liquid phase to the existing fluidised bed CFD model.

To produce sprays in fluidised bed coating processes, pneumatic or two-fluid atomisation is frequently used. In the mechanism of the two-fluid atomisation, as shown in Fig.1, a high velocity gas impacts a liquid jet issuing from a nozzle orifice creating high shear force over the liquid surface, leading to disintegration into spray droplets. The optimum frictional conditions resulting from high relative velocity between gas and liquid are generated by expanding the air to sonic or supersonic velocities before impacting the liquid (Hede *et al*., 2008). When injected from the nozzle orifice, the liquid jet starts to make contact with the mixing zone, expanding radially and squeezed into a thin circular sheet (Zeoli and Gu, 2006).

The term "liquid sheet" is used for both flat and cylindrical jets as common nomenclature (Hede *et al.,* 2008). For more details about two-fluid atomisation, the reader is referred to Hede *et al*. (2008), Sridhara and Raghunandan (2010) and Varga *et al*. (2003).

[Insert Figure 1 here]

Currently, to design and optimise the fluidised bed coating process, spray conditions and the operation of the two-fluid nozzle are identified as one of the most critical factors for the whole process and in practice have to be trial-and-error tested in order to control spray characteristics, including droplet size distribution, droplets trajectories and spray cone angle (Hede *et al*., 2008; Ronsse *et al*., 2007b). Therefore, in order to reduce time consumption and expensive cost of extensive experiments, many numerical approaches, for instance, Eulerian-Eulerian CFD, Eulerian-Lagrangian CFD, and population balance modelling, etc., have been developed as a powerful tool to comprehend or clarify the impact of different input variables on process efficiency and to research and design work (Ronsse *et al*., 2007b).

During the last few decades, CFD has been widely adopted in many industrial uses. In spray application, various numerical methods, for instance, the volume of fluid (VOF) method and the discrete phase method (DPM), have been developed to predict basic characteristics of spraying nozzles (e.g., spray angle and droplet size distribution) and to predict droplet trajectories. In the discrete phase method (Lagrangian framework), the droplet trajectory is calculated individually using the equation of motion, whereas the volume of fluid or multifluid method (Eulerian framework) is based on continuum mechanics which treat the two phases as interpenetrating continua (Taghipour *et al*., 2005).

For instance, for studying the two-fluid atomisation, instead of using only experimental PIV to provide an instantaneous map of the entire velocity field, Hoeg *et al*. (2008) used Eulerian CFD models to investigate the flow pattern of gas and liquid jets issuing from a two-fluid nozzle. In that work, good agreement between model-predicted and experimental data was found. Furthermore, Zeoli and Gu (2006) used the discrete phase model to simulate the critical droplet breakup during atomisation producing fine spherical metal powders. To verify their model performance, the liquid metal was initialised to large droplet diameters varying from 1 to 5 mm. They found that the model could provide quantitative assessment for the atomisation process. Pimentel *et al*. (2006) improved the capability of CFD models to capture liquid atomisation mechanisms of the two-fluid nozzle associated with the measured droplet diameters to initialise the droplet size in the discrete phase model. Even though many researchers have attempted to model droplet atomisation in various applications by means of CFD, as seen in Behjat *et al*. (2010), Fuster *et al*. (2009), Gianfrancesco *et al*. (2010), Kalata *et al*. (2009), Mezhericher *et al*. (2010), White *et al*. (2004) and Yamada *et al*. (2008), two-fluid atomisation occurring in the fluidised bed coating process still needs to be explored, considering the fact that the liquid is atomised in the presence of the fluidised solid phase.

In addition to the two approaches for modelling multiphase flow problems mentioned previously, the population balance model has been introduced to the CFD community as an alternative approach because of its reduced level of computational complexity (Aly *et al*., 2009). Moreover, the model can be easily coupled with the Eulerian-Eulerian model which eliminates the need for semi-empirical models employed in the Lagrangian framework (Aly *et al*., 2009). Recently, the population balance model has been extensively used in liquid-liquid and gas-liquid systems for modelling droplets and bubbles (Aly *et al*., 2010a, b). However, only few studies can be found in droplet atomisation problems, especially in fluidised bed coating systems. The atomisation process occurring in a plain jet air blast atomiser (two-fluid nozzle) was first investigated using the combination between a population balance model and a CFD Eulerian multi-fluid model by Aly *et al*. (2009). In that work, although the model obtained good agreement with experimental data, improvement still needed to be done. Therefore, Aly *et al*. (2010a, b) developed a new mathematical model for calculating droplet breakup frequency, instead of using a constant value, based on both drag and turbulence induced fragmentation stresses. Good agreement with the experimental data was achieved.

The main objective of this work is to present a CFD model of droplet atomisation of a two-fluid nozzle in the fluidised bed coating process, and to integrate it with existing gas-solid CFD models for fluidised bed coating processes as described by Duangkhamchan *et al*. (2010, 2011). Furthermore, the alternative numerical approach to describe two-fluid atomisation using population balance modelling combined with the Eulerian CFD framework is also demonstrated. Finally, the impact of process variables on spray characteristics and comparison of model-predicted distribution of voidage and liquid volume fraction obtained by two approaches are assessed.

The results presented in this paper are part of a research project aiming at modelling the complete top-spray fluidised bed coating process using CFD, with the global aim of understanding the process fundamentals and to provide the insight for optimising process control and reactor design. The modelling of the complete coating process requires several aspects to be studied in more detail and consequently, the research was split up into four parts, pertaining to the modelling of these aspects. First, a CFD model with appropriate selection of a drag model was constructed to allow the accurate prediction of gas/solid behaviour in tapered fluidised beds (Duangkhamchan *et al*., 2010). Next, the effect of the release of compressed air – to assist in the atomisation of the coating solution – on the hydrodynamic behaviour of the fluidised bed was studied (Duangkhamchan et al., 2011). The third part and also the subject of this research paper, deals with the hydrodynamic modelling of the liquid spray in the gas/solid fluidised bed. Finally, the overall CFD model will be concluded by adding the heat and mass transfer (i.e. evaporation of the binder solution in the droplets and as deposited onto the particles).

2. CFD model description

2.1. Discrete phase model (DPM)

In addition to solving transport equations for the continuous phases (i.e. gas and solids), a discrete phase of droplets was simulated in a Lagrangian framework. The trajectories of these discrete phase entities were computed individually. The coupling between the phases and its impact on both the discrete phase trajectories and the continuous phase flow was included.

2.1.1 The Euler – Lagrangian approach

In the Euler-Lagrangian approach, the gas and solid phases are treated as continuous phases by solving the time-averaged Navier-Stokes equations, while the dispersed phase (liquid phase) is solved by tracking a large number of droplets through the calculated flow field. The discrete phase can exchange momentum with the fluid phase.

<u>Continuous phase model</u>

Each volume within the mesh is simultaneously solved in an Eulerian frame of reference to obtain the gas flow field with the use of general conservation equations, as summarised below and described in more detail in Duangkhamchan *et al*. (2010, 2011).

The conservation of mass of phase *q* (*q* = either gas or solid) is described as

$$\frac{\partial}{\partial t}\left(\alpha_q \rho_q\right) + \nabla \cdot \left(\alpha_q \rho_q \vec{v}_q\right) = 0 \qquad (1)$$

where α_q is the phase volume fraction, ρ_q the density and $\vec{v}_q$ the velocity of phase *q*.

The following equation describes conservation of momentum for the fluid phase *l*:

$$\frac{\partial}{\partial t}\left(\alpha_l \rho_l \vec{v}_l\right) + \nabla \cdot \left(\alpha_l \rho_l \vec{v}_l \vec{v}_l\right) = -\alpha_l \nabla \cdot \tau_l + \alpha_l \rho_l \vec{g}_l + K_{ls}\left(\vec{v}_l - \vec{v}_s\right) \qquad (2)$$

In Eq. (2) is $\left(\vec{v}_l - \vec{v}_s\right)$ the slip velocity between the phases, where the subscript *l* denotes the fluid phase and *s* indicates the solid phase. K_{ls} denotes the drag force coefficient relevant to the phases *l* and *s*, *p* stands for the pressure and $\bar{\bar{\tau}}_l$ the deviatoric effective stress tensor of fluid phase.

<u>Discrete phase model</u>

The discrete phase model was solved in a Lagrangian frame of reference to simulate the spray pattern which is predicted by tracking the droplet trajectories by integrating the force balance of the particle (Newton's second law) (Behjat *et al*., 2010; Pimentel *et al*., 2006),

$$\frac{d\vec{v}_p}{dt} = \vec{F}_D + \frac{\vec{g}\left(\rho_p - \rho_p\right)}{\rho_p} \qquad (3)$$

where $\vec{F}_D$ is the drag force per unit particle mass,

$$\vec{F}_{\mathrm{D}} = \frac{3}{4} \cdot \frac{C_{\mathrm{D}} \rho_g}{\rho_{\mathrm{p}} d_p^2} \cdot \left| v_{\mathrm{g}} - v_{\mathrm{p}} \right| \cdot \left(\vec{v}_{\mathrm{g}} - \vec{v}_{\mathrm{p}} \right) \tag{4}$$

Here, $\vec{v}_{\mathrm{g}}$ is the gas phase velocity, $\vec{v}_{\mathrm{p}}$ is the droplet velocity, ρ_g is the gas density, ρ_p is the droplet density and d_p is the droplet diameter. C_D is the drag coefficient estimated using the correlation proposed by Morsi and Alexander (1972).

2.1.2 Air-blast/air-assisted atomiser model

Among the five atomiser models available in FLUENT, namely the plain-orifice, pressure-swirl, flat-fan, effervescent/flashing and air-blast/air-assisted atomiser models, the latter was found to be the suitable model for the two-fluid nozzle in this work due to similar atomisation mechanism. The air-blast/air-assisted atomiser model predicts droplet formation in those atomisers where an additional air stream is used to accelerate the breakup of the liquid sheet formed by the nozzle into droplets. In this case, droplet formation is characterised by the production of a liquid sheet, which further breaks up into ligands which finally disintegrate into droplets as shown in Figure 1.

In order to determine the liquid sheet thickness, the effective mass flow rate, $\dot{m}_{\mathrm{eff}}$, defined as

$$\dot{m}_{\mathrm{eff}} = \frac{2\pi \dot{m}}{\Delta\phi} \tag{5}$$

is used. In this equation, $\Delta\phi$ is the difference between the azimuthal stop angle and the azimuthal start angle, which was 2π for the nozzle type considered in this study (circular liquid sheet). Here, $\dot{m}$ is the liquid mass flow rate (kg s^{-1}) and hence, was equal to $\dot{m}_{\mathrm{eff}}$. Therefore, the thickness of sheet (mm), d_{sh}, produced by the air-blast/air-assisted atomiser can be approximated by relating the mass flow rate as

$$\dot{m}_{\mathrm{eff}} = \pi \rho_{\mathrm{l}} v_{\mathrm{l}} d_{\mathrm{sh}} \left(d_{\mathrm{inj}} - d_{\mathrm{sh}} \right) \tag{6}$$

where ρ_{l} is the liquid density (kg m^{-3}), v_{l} is the axial velocity component of the liquid at the nozzle orifice (m s^{-1}) and d_{inj} is the diameter of the liquid orifice. In Eq. (6), the effective mass flow rate is expressed as the liquid density (ρ_{l}) multiplied with the liquid velocity (v_{l}) and with the cross-sectional area of the circular liquid sheet with diameter ($d_{\mathrm{inj}} - d_{\mathrm{sh}}$) and sheet thickness d_{sh}.

Owing to the instability of the liquid sheet, the sheet breaks up and ligaments will be formed (Figure 1) whose length is given by

$$L_{\mathrm{lg}} = C_{\mathrm{sh}} \frac{v_{\mathrm{sh}}}{\Omega} \tag{7}$$

where L_{lg} is the ligament length (mm), C_{sh} denotes a sheet constant assumed to be responsible for sheet breakup, v_{sh} is the total velocity of the liquid sheet and Ω is the maximum growth rate (s^{-1}) and is found by numerically maximising the dispersion relation based upon the growth of sinuous waves on the liquid sheet (Schmidt *et al.*, 1999). For short waves, the ligament diameter is assumed to be linearly proportional to the wavelength that breaks up the sheet,

$$d_{\mathrm{lg}} = \frac{2\pi\, C_{\mathrm{lg}}}{K'} \quad (8)$$

where C_{lg} is the ligament constant, and K' is the wave number (m^{-1}) corresponding to the maximum growth rate, Ω. For more details concerning the air-blast/air-assisted atomiser model, the reader is referred to Ansys Inc. (2009b).

2.2 Multi-fluid flow model combined with population balance model (MFM-PBM)

In this approach, a conservation equation called the population balance equation is solved along with the Navier-Stokes equations in order to calculate the droplet diameter (Sauter Mean Diameter, SMD, which is commonly used to characterise droplets in spray modelling) and subsequent transport throughout the atomisation process. The population balance equation is a statement of continuity that describes how the statistical distribution of one or more droplet-related variables changes with time and space (Peglow *et al*., 2007). If the fraction of droplets with volume V at time t is given by the number density function $n(V, t)$, then the change in number of droplets with volume V as a result of larger droplets with volume V', fragmenting into droplets with volume V and the subsequent fragmentation of droplets with volume V into smaller droplets, is given in the population balance equation as (Ansys Inc., 2009a):

$$\frac{\partial}{\partial t}\left[n(V,t)\right] + \nabla \cdot \left[\vec{v}_{\mathrm{p}} n(V,t)\right] = \int_{V'} g(V')\beta(V/V')n(V',t)\,dV' - g(V)n(V,t) \quad (9)$$

In the above equation, only droplet fragmentation or break-up was considered while droplet coalescence was assumed to be negligible since sprays in the fluidised bed coating process are considered to be dilute. Furthermore, droplet breakup was assumed to be binary, i.e., when a droplet with volume *V*' breaks up, it forms two new droplets with volume *V* and (*V*'–*V*). The terms on the left hand side of Eq. (9) are the rate of change of the number density function and its convective derivative, respectively, while the terms on the right hand side represent the birth rate and the death rate terms resulting from droplet breakage (Ansys Inc., 2009a).

In Eq. (9) $g(V')$ is breakage frequency, being the fraction of droplets of volume *V*' breaking per unit time (s^{-1}) and β(V/V') is the droplet breakage kernel and expresses the probability that a droplet with volume *V* originates from the binary fragmentation of a droplet with volume *V*'. Hence, the first term on the right hand side of Eq. (9),

$$\int_{V'} g(V')\beta(V/V')n(V',t)dV' \tag{10}$$

represents the rate of formation, or birth rate, of droplets with volume *V* from breakage of droplets with volume *V*' ($V < V' < \infty$). The second term on the right hand side of Eq. (9),

$$g(V)n(V,t) \tag{11}$$

expresses the rate at which droplets with volume *V* disappear from the system due to fragmentation in smaller droplets, hence the term death rate.

Many methods, like for instance the Monte Carlo method (Lasheras *et al*., 2002; Ronsse *et al*., 2007a), the discrete method (Aly *et al*., 2009; Lasheras *et al*., 2002), the quadrature method of moments (Marchisio et al., 2003), and the direct quadrature method of moments (Madsen, 2006), are widely used in order to solve the population balance equations.

Due to the advantages of computing the droplet size distribution directly and the assumption of a small number of size intervals and the size distribution, in this work the discrete method (also known as the class method as referred to in this paper) was used to discretise the droplet population into a finite number of size intervals, *n*. In the class method, assuming that aggregation is negligible for dilute sprays, the population balance equation is written in terms of volume fraction of droplets with size class *i* (Aly *et al*., 2010; Aly *et al*., 2009):

$$\frac{\partial}{\partial t}\left(\rho_{\mathrm{p}}\alpha_{\mathrm{i}}\right)+\nabla\cdot\left(\rho_{\mathrm{p}}v_{\mathrm{i}}\alpha_{\mathrm{i}}\right)=\rho_{\mathrm{p}}V_{\mathrm{i}}\left(B_{\mathrm{i}}-D_{\mathrm{i}}\right) \qquad (12)$$

where V_{i} is the size of droplets in size class i, ρ_{p} is the density of the droplet phase and α_{i} is the volume fraction of droplet size class i defined as

$$\alpha_{\mathrm{i}} = N_{\mathrm{i}}V_{\mathrm{i}} \qquad i = 0,1,\ldots,n-1 \qquad (13)$$

where N_{i} is the total number of droplets per size class, and is given by

$$N_i = \int_{V_{\mathrm{i}}}^{V_{\mathrm{i+1}}} n(V)dV \qquad (14)$$

The droplet birth rate resulting from droplet breakage, B_{i}, and death rate term, D_{i}, in Eq.(12), are defined as

$$B_{\mathrm{i}} = \sum_{j=1}^{n} g(V_j)\beta(V_i/V_j)N_j \qquad (15)$$

$$D_i = g(V_i)N_i \qquad (16)$$

In this study, breakage kernel and breakage frequency in the death and birth rate terms in Eqs. (15) and (16) were similar to those used in Aly *et al*. (2009): the breakage kernel corresponded to a case where equal droplet fragments are distributed to all daughter size bins, while a constant frequency of 2000 Hz – a number corresponding to the reciprocal of the mean characteristic time scale of turbulence eddies – was chosen for the breakage frequency.

In order to solve the number density function, the population balance equation is linked to the Eulerian CFD model via a two-way coupling procedure. In this procedure, the velocity v_i is calculated in the Eulerian framework and then substituted into the population balance equation in order to compute the mean droplet sizes (SMD) which are then returned to the Eulerian solver to calculate the phase interaction such as the momentum exchange. Heat and mass transfer were not taken into account in this work.

3. Materials and methods

3.1. Overview of the numerical method

In this work, in addition to the discrete phase model (DPM) which has been widely used to describe droplet atomisation, the basic class method of population balance model combined with the multi-fluid phase model (MFM-PBM) was used to simulate the two-fluid atomisation. For both approaches, the 3-D geometry of a laboratory-scale Glatt GPCG-1 fluidised bed (Glatt GmbH, Germany) together with the two-fluid nozzle were meshed using Gambit 2.2.30 (Ansys Inc., Canonsburg, PA). A hybrid hexahedral-tetrahedral grid, containing 473 083 elements, was exported into the solver software, Ansys Fluent v.12 (Ansys Inc., Canonburg, PA). The grid is displayed in Fig. 2.

Flow turbulence was simulated using the standard k–ε model with standard wall functions, which has proven to result in good agreement with experimental data for this type of fluidised bed reactor geometry and solids material, as demonstrated in Duangkhamchan *et al*. (2010, 2011). First order upwind schemes were selected for the convection terms and the relation between velocity and pressure corrections was calculated using the phase-coupled SIMPLE algorithm.

In order to model the droplet atomisation and the droplets' interaction with the gas and solid phases, the numerical setup was separated into four sections corresponding to two approaches as follows:

- modelling droplet atomisation in a gas phase using the discrete phase model
- modelling droplet atomisation in a gas-solid flow by means of the discrete phase model combined with the multifluid flow model
- modelling droplet atomisation in a gas phase using the population balance model combined with the multifluid flow model
- modelling droplet atomisation in a gas-solid flow using the population balance model coupled with the multifluid flow model.

[Insert Figure 2 here]

3.2. Modelling the two-fluid atomisation using the DPM

3.2.1. Two-phase flow model (gas-liquid DPM model)

First, model parameters associated with the air-blast/air-assisted atomiser model were calibrated using published industrial data of the mean droplet diameter for the nozzle used in the Glatt GPCG-1 fluidised bed unit (Model 970-S1, Düsen-Schlick GmbH). In order to compare the calculated droplet sizes to the published industrial data, spray injections (water) at atomisation air pressures of 1.0 and 3.0 bar were simulated in a stagnant-air cylinder geometry.

Multiple simulations with variation of spray sheet thicknesses (d_{sh}) of 0.4, 0.7 and 1.0 mm, sheet constants (C_{sh}) of 14, 15 and 16, and ligament constants (C_{lg}) of 0.5, 0.7 and 0.9, were performed. After calibration of the air-blast atomiser model, the model was employed to study the atomisation in the geometry of the laboratory-scale fluidised-bed. Fluidisation air flow rates similar to those used in the previous works (Duangkhamchan *et al.*, 2010, 2011), namely 55, 76 and 97 m^3hr^{-1}, were selected. Other process variables are presented in Table 1.

[Insert Table 1 here]

3.2.2. Three-phase flow model (gas-solid-liquid DPM model)

A CFD model including all three phases and their interactions – i.e. momentum transfer – was developed to evaluate the impact of injection parameters. In this model, the water droplets were considered to be a separate phase in addition to the gaseous and solid particle phases in order to better describe the complex process of liquid spray inside the fluidised bed reactor. Interactions between gas and solid phases were solved in the Eulerian-Eulerian framework, including the modified-Gidaspow drag coefficient as employed in Duangkhamchan *et al*. (2010), while the trajectories of injected droplets were simulated by solving the equations of motion of individual dispersed phase entities. For fluidisation, the properties of 1 kg of glass beads were used (Depypere *et al*., 2009) as listed in Table 2, along with the boundary conditions and simulation parameters.

[Insert Table 2 here]

3.3. Modelling two-fluid atomisation using the MFM-PBM

3.3.1. Two-phase flow model (gas-liquid MFM-PBM model)

The unsteady pressure-based solver in Ansys Fluent v.12 was used with the Eulerian multiphase model coupled with the discrete population balance model in order to simulate water droplet atomisation through the two-fluid nozzle. Assuming that sprays are dilute, turbulence was modelled using the dispersed k-ε turbulence model. To ensure solution convergence behaviour within each time step, a small time step of 10^{-5} s was chosen. The velocity boundary conditions for water and atomising air are shown in Table 1. As the use of compressed air in the two-fluid nozzle produces droplets with a size ranging from 10 to 40 µm (Lefebvre, 1989), in this work, the droplet population was discretised into 7 size classes with a diameter ranging from 10 to 40 µm. The breakage kernel was computed to represent a case where droplet fragments are distributed to all daughter size bins.

3.3.2. Three-phase flow model (gas-solid-liquid MFM-PBM model)

Instead of solving the motion of injected droplets separately in the Lagrangian discrete phase model, the gas, droplets and solid particles were treated as interpenetrating continua in the Eulerian framework. The gas phase was considered to be the primary phase, whereas the droplets and solid particle phases were the secondary phases. To track the droplet diameter in the Eulerian solver, the number density function was solved using the class population balance method (see Section 2.2).

3.4. Experimental spray visualisation

3.4.1. Measurement set-up

Spray visualisation experiments were performed in a transparent, polycarbonate reactor with similar dimensions to the Glatt GPCG-1 fluidised bed coating reactor. The tapered reactor had a bottom diameter of 0.15 m, a top diameter of 0.30 m and a total height of 0.56 m. The reactor shell material consisted of 5 mm thick polycarbonate. Fluidisation air was provided by a 2.2 kW high pressure centrifugal fan (Ventomatic CHT160-2T-3, Belgium) equipped with electronic frequency control (Figure 3). The volumetric air flow rate was measured between the fan and the reactor inlet by means of a 0.1 m diameter rotating vane flow meter (Airflow Developments, VMD20, UK).

The air distributor used in the fluidised bed reactor consisted of a Robusta 172×36 wpi (wires per inch) wire mesh (Spörl KG, Germany). The pneumatic nozzle (Schlick Model 970-S1, Germany), normally used in the Glatt GPCG-1, was installed in the lower nozzle port of the transparent reactor. The spraying liquid was water with an added fluorescent dye, being sodium fluorescein salt (Sigma-Alldrich) and was transported to the pneumatic nozzle by means of a peristaltic pump (Watson-Marlow, 505 Du/RL, US).

The spray cone produced by the pneumatic nozzle was visualized by means of UV illumination by directing a 400 W UV spotlight 0.5 m above the reactor outlet. Illumination through the open reactor outlet proved to be most efficient, as the polycarbonate reactor shell material had some UV absorbing capacity. The illuminated spray was recorded by a digital camera (Olympus i-Speed 1) at 60 fps (800 × 600 pixel size), and stored in an uncompressed video format (AVI).

[Insert Figure 3 here]

3.4.2. Data processing

To visualise the spray cone, post-processing of the captured image data was necessary (i.e. contrast enhancement). The uncompressed frames captured by the video camera can be considered to be matrices holding the pixel intensity values (between 0 and 1), A_i, with subscript i indicating the frame number (i.e. 60 per recorded second of video) and having dimensions of 800 by 600. As the recording is triggered at the moment of activating the peristaltic pump, an initial number of frames, b, is recorded without spray, i.e., before the development of the actual spray cone. Of these b frames, an average, A'_b, is calculated which serves as a reference blank frame which will be subtracted from the actual spraying frames,

$$A'_\mathrm{b} = \frac{1}{b}\sum_{i=1}^{b} A_\mathrm{i} \tag{17}$$

The actual frames to be used for visualisation were taken after the steady-state spraying cone had developed, which are denoted by frames A_i with $m \leq i \leq n$. The contrast enhancement of each of the frames during steady-state spraying consisted of two steps. First, the reference blank frame was subtracted from the spraying frame A_i resulting in A''_i, and second, each frame matrix was multiplied with a scalar so the pixel with the highest intensity value in A_i reached unity (i.e. maximum intensity) – with the new resulting matrix denoted as E_i:

$$m \leq i \leq n \rightarrow \begin{cases} A''_\mathrm{i} = A_\mathrm{i} - A'_\mathrm{b} \\ E_\mathrm{i} = x \cdot A''_\mathrm{i} \Leftrightarrow \max\left(E_\mathrm{i}\right) = 1 \end{cases} \tag{18}$$

Finally, the average matrix of all E_i with $m \leq i \leq n$ was taken and used as the contrast-enhanced spray visualisation image,

$$E' = \frac{1}{n-m}\sum_{m}^{n} E_{\mathrm{i}} \qquad (19)$$

4. Results and Discussion

4.1. Air-blast/air-assisted atomiser model calibration

Several simulations with different spray injection setups were performed in order to calibrate the air-blast atomiser model as outlined in Section 3.2.1. The measured mean volume droplet diameters at 1.0 and 3.0 bar atomisation pressure (data supplied by Düsen-Schlick GmbH) were compared with simulated mean droplet sizes while the ligament constant, the sheet constant and sheet thickness were varied.

Figure 4 shows the simulated versus experimental mean droplet sizes at 3.0 bar atomisation pressure and using different values for the ligament constant, C_{lg}. It can be observed that the spray injection characterised by using a ligament constant, C_{lg} of 0.9, gave the best agreement with the experimental mean droplet diameter. With respect to variation of the sheet constant (C_{sh}) and the sheet thickness (d_{sh}), no significant differences in model-predicted droplet diameter distribution were observed. Similar trends were seen from simulations with 1.0 bar atomisation pressure and consequently, the following calibrated air-blast atomiser model parameters were used in subsequent simulations: Ligament constant, $C_{\mathrm{lg}} = 0.9$ and standard values for sheet constant, $C_{\mathrm{sh}} = 15$ and sheet thickness, $d_{\mathrm{sh}} = 0.7$ mm.

[Insert Figure 4 here]

4.2. Two-phase (gas-liquid) model of droplet atomisation in the fluidised bed coater

4.2.1. Discrete phase model (gas-liquid DPM)

Using calibrated atomiser model parameters, the spray was modelled using DPM inside the geometry of a fluidised bed coater, as detailed in Table 2 and Figure 2. The effects of fluidisation air flow rate, atomisation air pressure and liquid feed rate – as outlined in Table 1 – on spray characteristics were simulated.

Figure 5 demonstrates the contour plots of droplet mass fraction at different atomisation air pressures. It can be seen that the spray pattern did not change with increasing atomisation air pressure. When considering the impact of fluidisation air flow rate, as detailed in Figure 6, higher flow rates were seen to reduce the diameter of the spray cone and to lower the droplet mass fraction in the reactor. This can be explained by the fact that, at higher fluidisation air flow, droplets are easier lifted out of the reactor. However, it is important to stress that the DPM model in its current state did not include droplet evaporation (no energy equation). Consequently, the length of model-predicted droplet trajectories is likely to be overestimated compared to the actual process, where droplets are subjected to spray drying. Finally, the effect of liquid feed rate on the droplet mass fraction distribution is shown in Figure 7. At higher liquid feed rates, more droplets can be produced. Due to the higher amount of spray issuing from the nozzle in Figure 7c, the spray cone shape can obviously not be characterised.

[Insert Figure 5 here]

[Insert Figure 6 here]

[Insert Figure 7 here]

4.2.2. Multi-fluid flow model combined with population balance model (gas-liquid MFM-PBM)

Figure 8 shows the distribution of the Sauter mean droplet diameter (SMD) and droplet volume fraction in the geometry of the fluidised bed coater, as predicted by the MFM-PBM gas-liquid model under reference scenario conditions as outlined in Table 1. From this figure, it can be observed that the mean droplet sizes decreases continuously as the droplets depart from the liquid orifice of the nozzle until they reach the air distributor.

[Insert Figure 8 here]

Comparison of the droplet volume fraction as shown in Figure 8b with the droplet mass fraction from the DPM model gives a moderately good agreement (same order of magnitude if mass fraction is converted to volume fraction). The exception is a more narrow spray cone that was predicted by the MFM-PBM model. Furthermore, as the droplets were treated as a continuum in the MFM-PBM model, the droplet phase was seen to deflect from the air distributor at the bottom of the reactor (Figure 8b). This effect is not visible as such in the DPM results (Figure 5b), because in the DPM algorithm, droplet tracking was ended when a droplet impacted on the boundaries of the reactor geometry. Given these results, the MFM-PBM can be opted for as an alternative approach to model the atomisation of the two-fluid nozzle, considering advantages including minimum level of computational complexity, ease of coupling with the Eulerian-Eulerian CFD model and eliminating the need for semi-empirical models employed in the DPM model (Aly *et al*., 2009).

Simulations with varying liquid feed rate, atomisation air pressure and fluidisation air flow rate were also performed. However, significant differences in droplet size distribution were not predicted by the MFM-PBM model with respect to process condition dependency. This observation is not consistent with both numerical and experimental studies reported in literature (Hede *et al*., 2008; Lal *et al*., 2010; Lebas *et al*., 2009; Liao and Lucas, 2009; Liu *et al*., 2006; Sridhara and Raghunandan, 2010). The possible explanation of this inconsistency is the assumption of a constant breakage kernel and breakage frequency in this study. In reality, breakage depends on droplet properties including size, as well as on local turbulences in the flow field. Consequently, improvement in model accuracy of the MFM-PBM model could be achieved if the breakage frequency and kernel are made dependant on (i.e. 'sensitised to') the droplet Weber and local Reynolds numbers (Aly *et a*l., 2009; Aly *et al*., 2010a, b).

4.3. Spray pattern validation (gas-liquid two-phase flow)

Spray visualisation images combined with UV illumination as a function of atomisation air pressure are presented in Fig. 9. The effect of fluidisation air flow rate, varied within the interval outlined in Table 1, showed no observable difference in spray pattern. Regarding atomisation air pressure, higher air pressure not only resulted in a narrower spraying cone, but also resulted in a slightly asymmetric spraying cone, as shown in Fig. 9d. The asymmetry is likely due to the higher volume of expanding atomisation air (for P_{at} = 3 bar) in combination with the asymmetric construction of the reactor resulting from the one-sided nozzle support (not shown in Fig. 9).

[Insert Figure 9 here]

When the experimental results are compared with the model-predicted spray patterns, a qualitative agreement was obtained with the DPM or MFM-PBM predicted results. However, DPM gave better agreement compared to MFM-PBM including a wider spraying cone and much less deflection of the spray at the base of the reactor. As already stated in Section 4.2.2., as opposed to the MFM-PBM, the DPM can effectively account for droplet-wall collisions which corresponds with the actual (experimental) process, where most of the droplets were seen to adhere onto the wire mesh air distributor at the base of the reactor.

4.4. Three-phase (gas-solid-liquid) model of droplet atomisation in the fluidised bed coater

4.4.1. Discrete phase model (gas-solid-liquid DPM)

Figure 10a shows the contour plot of the time-averaged steady-state voidage, taken over a simulated time period of 10s. The initial 5s of the simulated process were discarded to avoid the start-up fluidisation behaviour. As can be observed in Fig. 10a, in the central part of the reactor, the region under the nozzle is occupied by the hollow atomisation cone. In this zone, the solid particles have to be lifted by the fluidising air against the counterforce of the atomisation air resulting in a voidage (Duangkhamchan *et al*., 2011), while a denser zone can be noticed in a radial area between the nozzle atomisation air cone and the reactor walls. It could be explained that particles move predominantly upwards in the centre to the above bed region (about 12 cm high above the air distributor), then move radially towards the walls and downwards along the walls. This particle flow behaviour was confirmed by experimental results obtained by Positron Emission Particle Tracking (PEPT) (Depypere *et al*., 2009).

[Insert Figure 10 here]

Fig. 10b confirms that the contacting between the droplet and fluidising particles occurs at the central part of the vessel. Fig. 10b demonstrates the droplets tracked at 15s. The calculated droplet tracks revealed that droplets moved downwards along with the atomisation air cone until facing the counter-current fluidising solid particles. Considering the absence of phenomena including droplet evaporation and droplet/solids adhesion, the DPM algorithm continues to track the droplets until they exit the reactor at the top or impact one of the reactor geometry boundaries. In reality, the majority of the droplets adhere onto the fluidised particles, contributing to the layered growth of the coating wall around the individual core particles. Also, in an actual fluidised bed coating process, the majority – typically ≥ 70 % (Ronsse *et al*., 2008) – of water in the coating solution is evaporated after the droplets have impacted the surface of the fluidised core particles. Only a minority of the water is evaporated during droplet travel between the nozzle and the impacting particle surface. Consequently, there will be a minimal impact of the droplet size reduction as a result of droplet drying on the droplet dynamics (i.e. altered drag force, reduced droplet mass) and the resulting droplet trajectories.

4.4.2. Multi-fluid flow model combined with population balance model (gas-solid-liquid MFM-PBM)

Comparison between the gas-solid-liquid phase DPM and MFM-PBM model-predicted results is shown in Figure 10a-d. As can be seen in Fig. 10a and 10c, the model-predicted time-averaged steady-state voidage profiles of both models have a strong agreement. Also, when considering the model-predicted distribution of droplets within the fluidised bed (Figs. 10b and 10d), and specifically the penetration depth of the droplets in the bed, the MFM-PBM predicted results are consistent with those from the DPM.

5. Conclusions

As a powerful numerical tool for solving fluid flow problems, CFD was used to model the important aero- and hydrodynamic aspects of a fluidised bed coater, including the gas, liquid, and solid phases using two approaches: Eulerian-Lagrangian and combined Eulerian-Eulerian/population balance model. In the discrete phase model (DPM), the calibrated air-blast/air-assisted atomiser model was used as and the effects of process variables on spray flow and its mass distribution were studied. It was, in the gas-liquid DPM model, that the spray cone and liquid mass fraction change with the variation of fluidisation air flow rate, atomisation air pressure and liquid feed rate.

The population balance model combined with the Eulerian-Eulerian CFD model was employed as an alternative approach to describe the two-fluid atomisation and the impact of process variables. The gas, droplets and solid particles were modelled by treating all phases as interpenetrating continua in the Eulerian framework, while the class population balance model was used to track the droplet diameter. The simulated results showed that even though this approach could be opted for instead of the DPM model to capture the two-fluid atomisation and interaction between phases, improvement of the population balance model by for instance including more accurate breakage kernels (i.e. depending on Weber and Reynolds numbers) has to be carried out. When evolving from a gas-liquid to a gas-solid-liquid CFD model, consistency between the DPM and the population balance model in the Eulerian framework was shown to improve. Consequently the MFM-PBM approach was considered to be a viable alternative in the CFD modelling of gas-solid-liquid systems, including fluidised bed coaters.

Finally, given the absence of thermodynamics in the presented model, effects such as droplet evaporation could not be captured with the CFD model in its current state. Future work will comprise the addition of the energy equation for the description of heat transfer phenomena, as well as droplet evaporation and to tie together all phenomena occurring in the gas-liquid-solid multiphase system into a single comprehensive CFD model, suitable for accurately describing fluidised bed coating processes with the aim of improving process understanding and optimising the coating process in terms of process conditions and reactor design.

Nomenclature

A, *A*’, *A*”, *E*	Image intensity matrices
B	Birth rate, s^{-1}
C	Constant
D	Death rate, s^{-1}
d	diameter, m
F	Force per unit mass, N kg^{-1}
$\vec{g}$	Acceleration due to gravity, m s^{-2}
g( )	Breakage frequency, s^{-1}
K	Interphase momentum exchange coefficient, kg $m^{-3}s^{-1}$
K’	Wave number corresponding to the maximum growth rate, m^{-1}
L	Length, m
$\dot{m}$	Mass flow rate, kg s^{-1}
n( )	Number density function
p	pressure, Pa
Re	Reynolds number, dimensionless
t	Time, s
v	velocity, m s^{-1}
V, *V*’	Volume, m^3
$\dot{V}$	Volumetric flow rate, m^3s^{-1}
x	Scalar

Greek symbols

α	Volume fraction, dimensionless
β( )	Probability density function, kernel function

ρ	Density, kg m^{-3}
τ	Deviatoric stress tensor, kg m^{-1}s^{-2}
μ	Dynamic viscosity of gas, kg m^{-1}s^{-1}
ϕ	Angle, rad
Ω	Maximum grow rate, s-1

Subscripts

at	atomisation
q	solid or gas phase
b	initial
D	drag
eff	effective
f	fluidisation
g	gas phase
i	class or integer
inj	injector exit
l	fluid phase
s	solid phase
lg	ligament
p	particle or droplet
sh	sheet

References

Aly, H.S., Eldrainy, Y.A., Lazim, T.M., Jaafar, M.N.M., 2010a. On the contribution of drag and turbulent stresses in the fragmentation of liquid droplets: A Computational Study. CFD Letters 2 (2), 97-105.

Aly, H.S., Eldrainy, Y.A., Saqr, K.M., Lazim, T.M., Jaafar, M.N.M., 2010b. A mathematical model for predicting spray atomisation characteristics in an Eulerian-Eulerian framework. International Communications in Heat and Mass Transfer 37, 618-623.

Aly, H.S., Lazin, T.M., Eldrainy, Y.A., Jaafar, M.N.M., 2009. Mathematical modelling of droplet atomisation using the population balance equation. International Conference on Signal Processing Systems, ICSPS 2009. Institute of Electrical and Electronics Engineers, New York, 955-959.

Ansys Inc., 2009a. Ansys Fluent 12.0 Population balance module manual. Ansys Inc., Canonsburg, PA.

Ansys Inc., 2009b. Ansys Flent 12.0 User's guide manual. Ansys Inc., Canonsburg, PA.

Behjat, Y., Shahhosseini, S., Marvast, M.A., 2010. Modeling gas oil spray coalescence and vaporisation in gas solid riser reactor. International Communications in Heat and Mass Transfer 37, 935-943.

Depypere, F., Pieters, J.G., Dewettinck, K., 2009. PEPT visualisation of particle motion in a tapered fluidised bed coater. Journal of Food Engineering 93 (3), 324-336.

Duangkhamchan, W., Ronsse, F., Depypere, F., Dewettinck, K., Pieters, J.G., 2010. Comparison and evaluation of interphase momentum exchange models for simulation of the solids volume fraction in tapered fluidised beds. Chemical Engineering Science 65, 3100-3112.

Duangkhamchan, W., Ronsse, F., Dewettinck, K., Pieters, J.G., 2011. CFD study of solids concentration in a fluidised bed coater with variation of atomisation air pressure. Powder Technology 212, 103-114.

Duesen-Schlick GmbH, Technical information 15/01, Duesen-Schlick GmbH, Coburg, Germany.

Fuster, D., Bague, A., Boeck, T., Moyne, L.L., Leboissetier, A., Popinet, S., Ray, P., Scardovelli, R., Zaleski, S., 2009. Simulation of primary atomisation with an octree adaptive mesh refinement and VOF method. International Journal of Multiphase Flow 35, 550-565.

Gianfrancesco, A., Turchiuli, C., Flick, D., Dumoulin, E., 2010. CFD Modeling and Simulation of Maltodextrin Solutions Spray Drying to Control Stickiness. Food Bioprocess Technology 3(6), 946-955.

Hede, P.D., Bach, P., Jensen, A.D., 2008. Two-fluid spray atomisation and pneumatic nozzles for fluid bed coating/agglomeration purposes: A review. Chemical Engineering Science 63, 3821-3842.

Hoeg, D.P., Wang, Z., Friedman, P.D., Laoulache, R.N., 2008. Investigation of a coaxial air-blast atomiser using particle image velocimetry and computational fluid dynamics. Atomisation and Sprays 18, 739-759.

Kalata, W., Brown, K., Bade, K.M., Schick, R.J., 2009. Dimensional, thermal and evaporative Spray plume characteristics using Computational Fluid Dynamics, simulation versus empirical evaluation. Spray Analysis and Research Services, A Service of Spraying Systems Co., Wheaton, USA.

Lal, S., Kushari, A., Kapoor, J.C., Maji, S., 2010. Modelling of externally mixed air blast atomiser. International Journal of Dynamics of Fluids 6(1), 25-40.

Lasheras, J.C., Eastwood, C., Martinez-Bazaan, C., Montanes, J.L., 2002. A review of statistical models for the break-up of an immiscible fluid immersed into a fully developed turbulent flow. International Journal of Multiphase Flow 28, 247-278.

Lebas, R., Menard, T., Beau, P.A., Berlemont, A., Demoulin, F.X., 2009. Numerical simulation of primary break-up and atomisation: DNS and modelling study. International Journal of Multiphase Flow 35, 247-260.

Lefebvre, A.H., 1989. Atomisation and sprays. Hemisphere Publishing Corporation, Washington, DC.

Liao, Y., Lucas, D., 2009. A literature review of theoretical models for drop and bubble breakup in turbulent dispersions. Chemical Engineering Science 64, 3389-3406.

Liu, H.F., Li, W.F., Gong, X., Cao, X.K., Xu, J.L., Chen, X.L., Wang, Y.F., Yu, G.S., Wang, F.C., Yu, Z.H., 2006. Effect of liquid jet diameter on performance of coaxial two-fluid airblast atomisers. Chemical Engineering and Processing 45, 240-245.

Madsen, J., 2006. Computational and experimental study of sprays from the breakup of water sheets. Ph.D. Thesis, Faculty of Engineering and Science, Aalborg University, Esbjerg, Denmark.

Marchisio, D.L., Pikturna, J.T., Fox, R.O., Vigil, R.D., 2003. Quadrature method of moments for population balance equations. AIChE Journal 49, 1266-1276.

Mezhericher, M., Levy, A., Borde, I., 2010. Spray drying modelling based on advanced droplet drying kinetics. Chemical Engineering and Processing: Process Intensification 49, 1205-1213.

Morsi, S.A., Alexzander, A.J., 1972. An investigation of particle trajectories in two-phase flow systems. Journal of Fluid Mechanics 55, 193–208.

Peglow, M., Kumar, J., Heinrich, S., Warnecke, G., Tsotsas, E., Mörl, L., Wolf, B., 2007. A generic population balance model for simultaneous agglomeration and drying in fluidized beds. Chemical Engineering Science 62, 513-532.

Pimentel, R.G., de Champlain, A., Kretschmer, D., Stowe, R.A., Harris, P., Kurbatskii, K., 2006. Improved atomization model for CFD codes. Proceeding of the International Conference on Liquid Atomisation and Sprays Systems, Kyoto, Japan.

Ronsse, F., Pieters, J.G., Dewettinck, K., 2007a. Combined population balance and thermodynamic modelling of the batch top-spray fluidised bed coating process. Part I-Model development and validation. Journal of Food Engineering 78, 296-307.

Ronsse, F., Pieters, J.G., Dewettinck, K., 2007b. Numerical spray model of the fluidised bed coating process. Drying Technology 25, 1491-1514.

Ronsse, F., Pieters, J.G. & Dewettinck, K., 2008. Modelling side-effect spray drying in top-spray fluidised bed coating processes. Journal of Food Engineering, 86, 529-541.

Salman, A.D., Hounslow, M.J., Seville, J.P.K., 2007. Handbook of Powder Technology, Vol. 11: Granulation. Elsevier Publishing, Amsterdam.

Schmidt, D. P., Nouar, I., Senecal, P. K., Rutland, C. J., Martin, J. K., and Reitz, R. D., 1999. Pressure-swirl atomisation in the near field. SAE Transactions, Journal of Engines 108(3), 471-484.

Spray Drying Systems Co., 2000. Engineer’s guide to spray drying technology.

Sridhara, S.N., Raghunandan, B.N., 2010. Photographic investigations of jet disintegration in airblast sprays. Journal of Applied Fluid Mechanics 3(2), 111-123.

Taghipour, F., Ellis, N., Wong, C., 2005. Experimental and computational study of gas-solid fluidised bed hydrodynamics. Chemical Engineering Science 60, 6857-6867.

Teunou, E., Poncelet, D., 2002. Batch continuous fluid bed coating – review and state of the art. Journal of Food Engineering 53, 325-340.

Varga, C.M., Lasheras, J.C., Hopfinger, E.J., 2003. Initial breakup of a small-diameter liquid jet by a high-speed gas stream. Journal of Fluid Mechanics 497, 405-434.

White, T.R., Milton, B.E., Behnia, M., 2004. Direct injection of natural gas/liquid diesel fuel sprays. Proceeding of the 15th Australasian Fluid Mechanics Conference, Sydney, Australia.

Yamada, H., Yoon, G., Okumiya, M., Okuyama, H., 2008. Study of Cooling System with Water Mist Sprayers: Fundamental Examination of Particle Size Distribution and Cooling Effects. Building Simulation 1(3), 214-222.

Zeoli, N., Gu, S., 2006. Numerical modelling of droplet break-up for gas atomisation. Computational Materials Science 38, 282-292.

List of Tables and Figures

atomisation air pressures: 1.0 bar (a-c) and 3.0 bar (d-e). Boundaries are indicated with ‘w’ for reactor walls, ‘d’ for air distributor and ‘n’ for nozzle.

Figure 10. Comparison between (a) contour of gas-solid-liquid DPM model-predicted time-averaged steady-state voidage, (b) gas-solid-liquid DPM model-predicted droplet tracks at *t* = 15s, (c) contour of gas-solid-liquid MFM-PBM model-predicted time-averaged steady-state voidage and (d) contour of gas-solid-liquid MFM-PBM model-predicted time-averaged steady-state liquid volume fraction.

Table 1. Process variables used in this study ([a] indicates reference scenario).

Table 2. Boundary conditions and simulation parameters.

Figure 1. Schematic overview of the two-fluid nozzle (a) and the mechanism of droplet atomisation (b), adapted from Salman *et al*. (2007) and Spray Drying Systems Co. (2000).

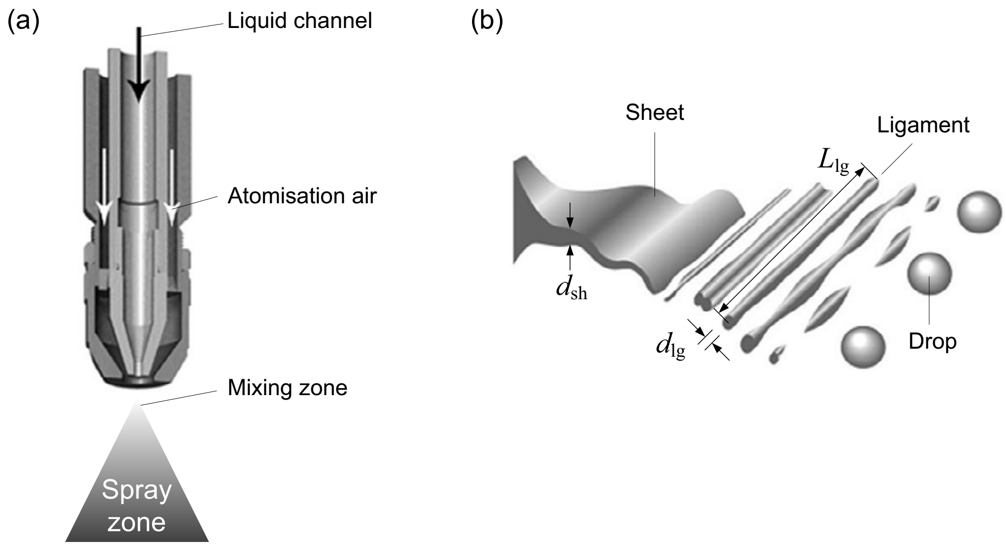

Figure 2. Meshed geometry of a conical Glatt GPCG-1 reactor together with the two-fluid nozzle.

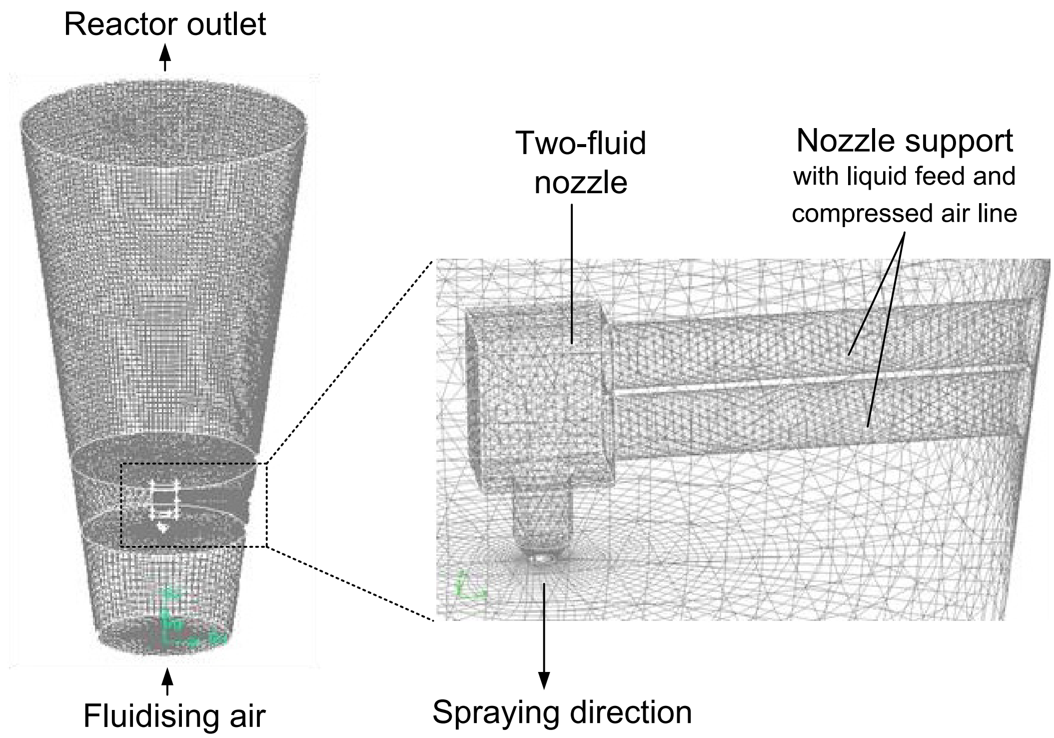

Figure 3

Figure 3. Spray visualisation setup.

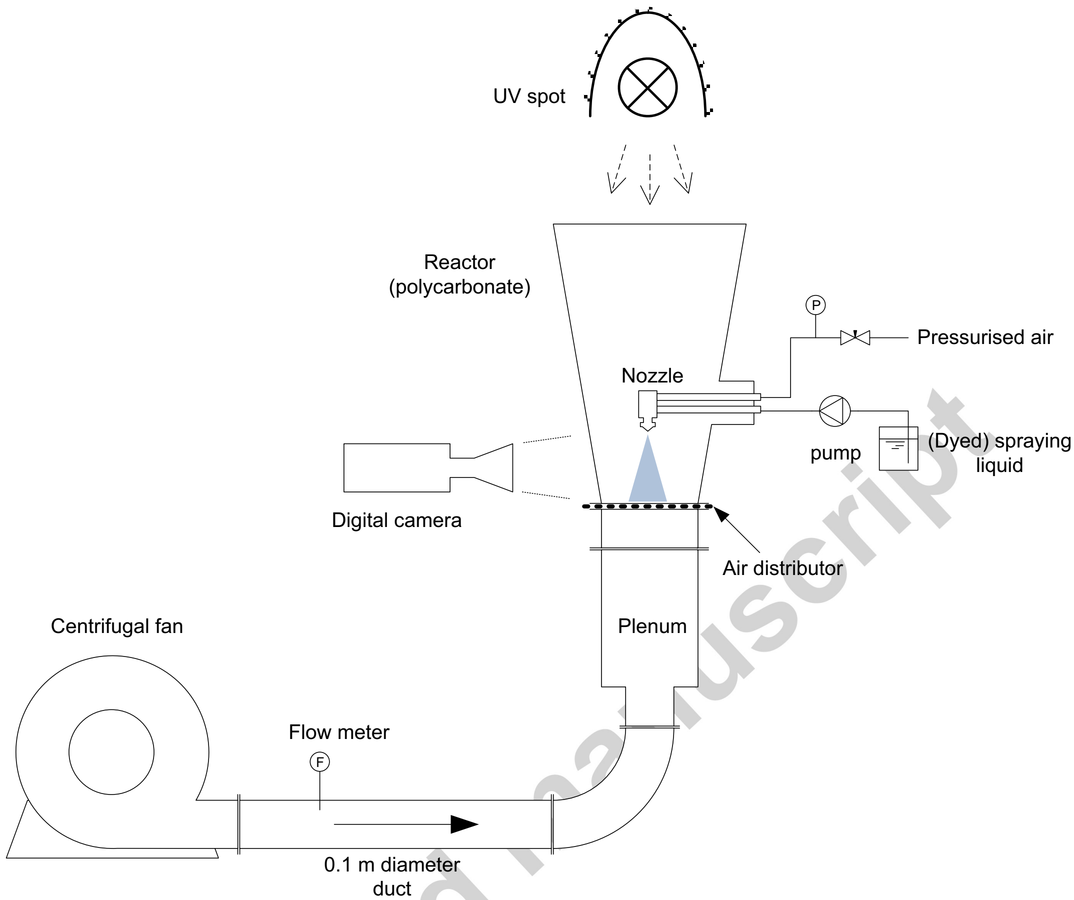

Figure 4

Figure 4. Effect of ligament constant, C_{lg}, on the model-predicted mean volume droplet diameter, compared against the experimental droplet size, as provided by Düsen-Schlick.

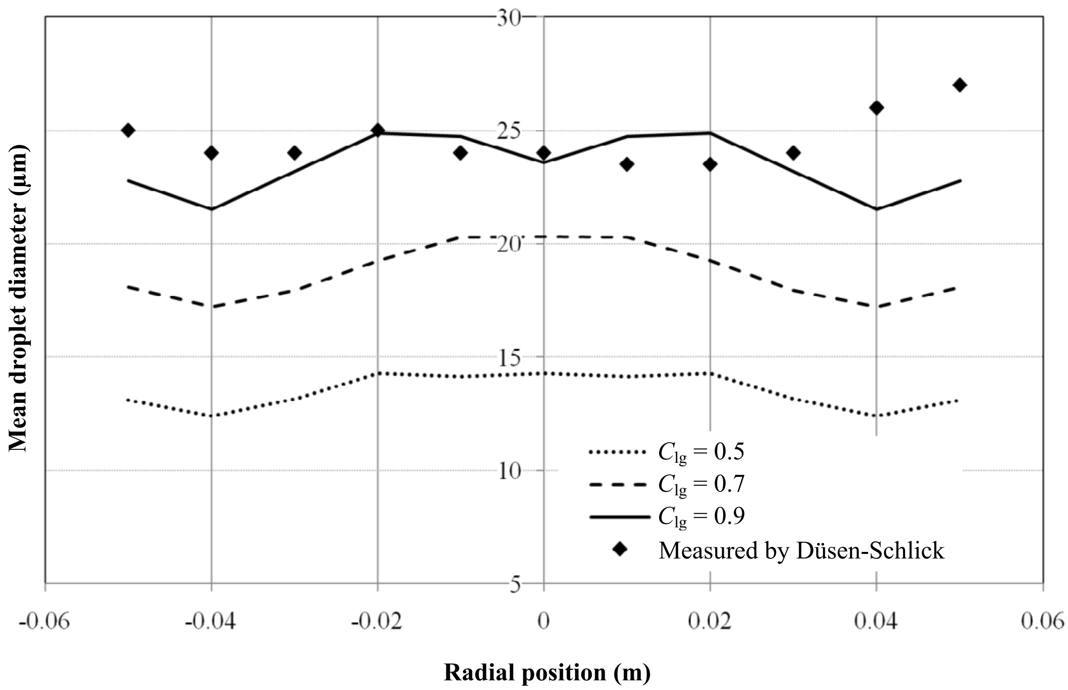

Figure 5

Figure 5. Contour plots of model-predicted (gas-liquid DPM) droplet mass fractions at atomisation air pressures of (a) 1.0 bar, (b) 2.0 bar (reference scenario, see Table 1) and (c) 3.0 bar.

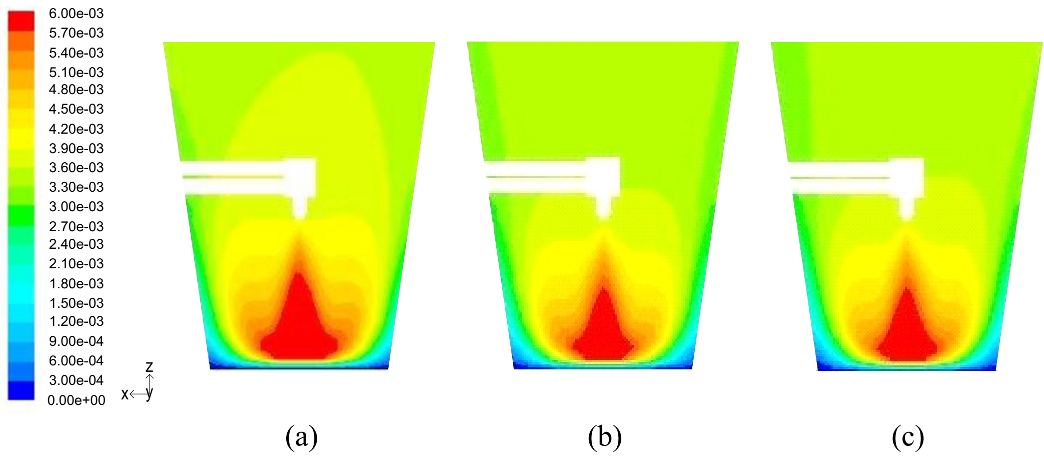

Figure 6. Contour plots of model-predicted (gas-liquid DPM) droplet mass fractions at fluidisation air flow rates of (a) 55 m^3hr^{-1}, (b) 76 m^3hr^{-1} (reference scenario, see Table 1) and (c) 97 m^3hr^{-1}.

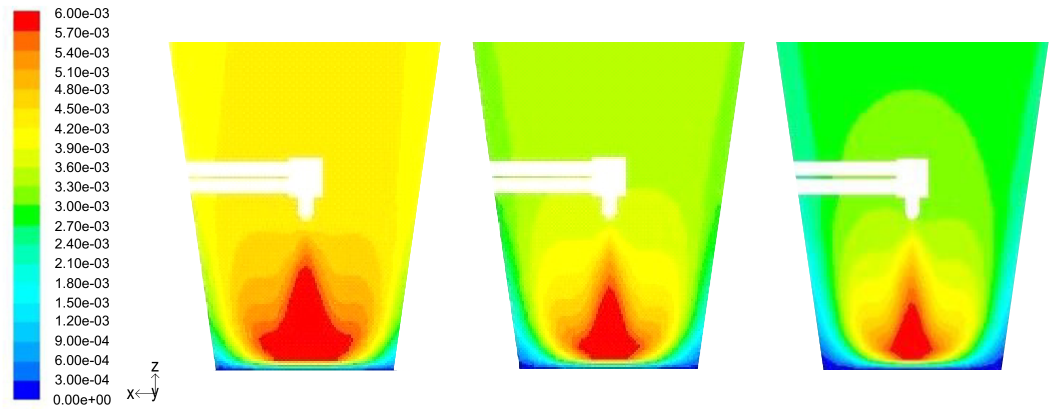

(a) (b) (c)

Figure 7. Contour plots of model-predicted (gas-liquid DPM) droplet mass fractions at liquid feed rates of (a) 0.5×10^{-4} kg s^{-1}, (b) 1.0×10^{-4} kg s^{-1} (reference scenario, see Table 1) and (c) 1.5×10^{-4} kg s^{-1}.

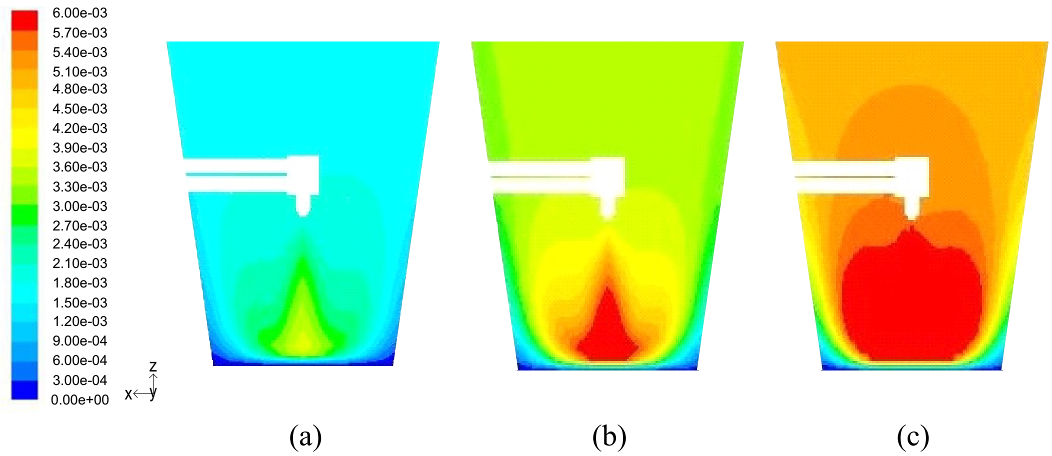

Figure 8. Simulated distribution of the droplet Sauter mean diameter, in m (a) and droplet volume fraction (b) using reference scenario conditions, as outlined in Table 1, as predicted by the gas-liquid MFM-PBM model.

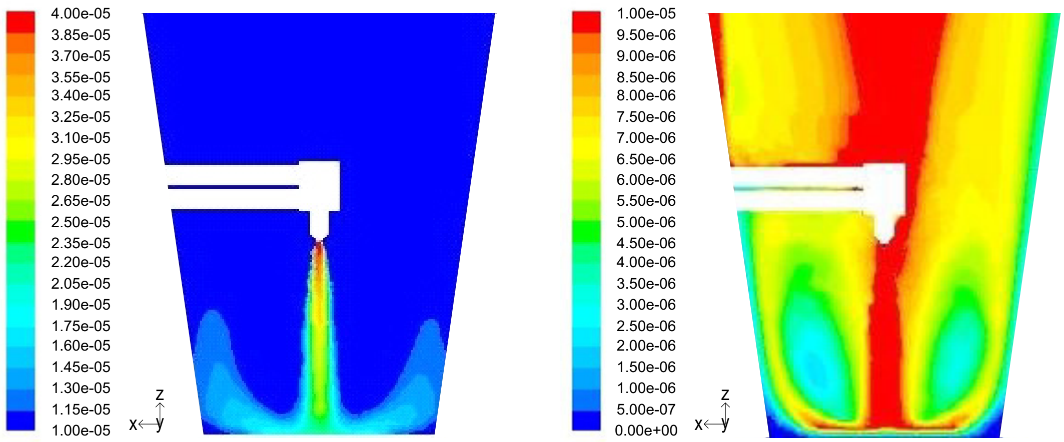

(a) (b)

Figure 9. Comparison of the visualised spray pattern (a, d) with the gas-liquid PBM model-predicted mass fraction contours (b, e) and with the gas-liquid MFM-DPM model-predicted volume fraction contours (c, f). Results plotted for two atomisation air pressures: 1.0 bar (a-c) and 3.0 bar (d-e). Boundaries are indicated with 'w' for reactor walls, 'd' for air distributor and 'n' for nozzle.

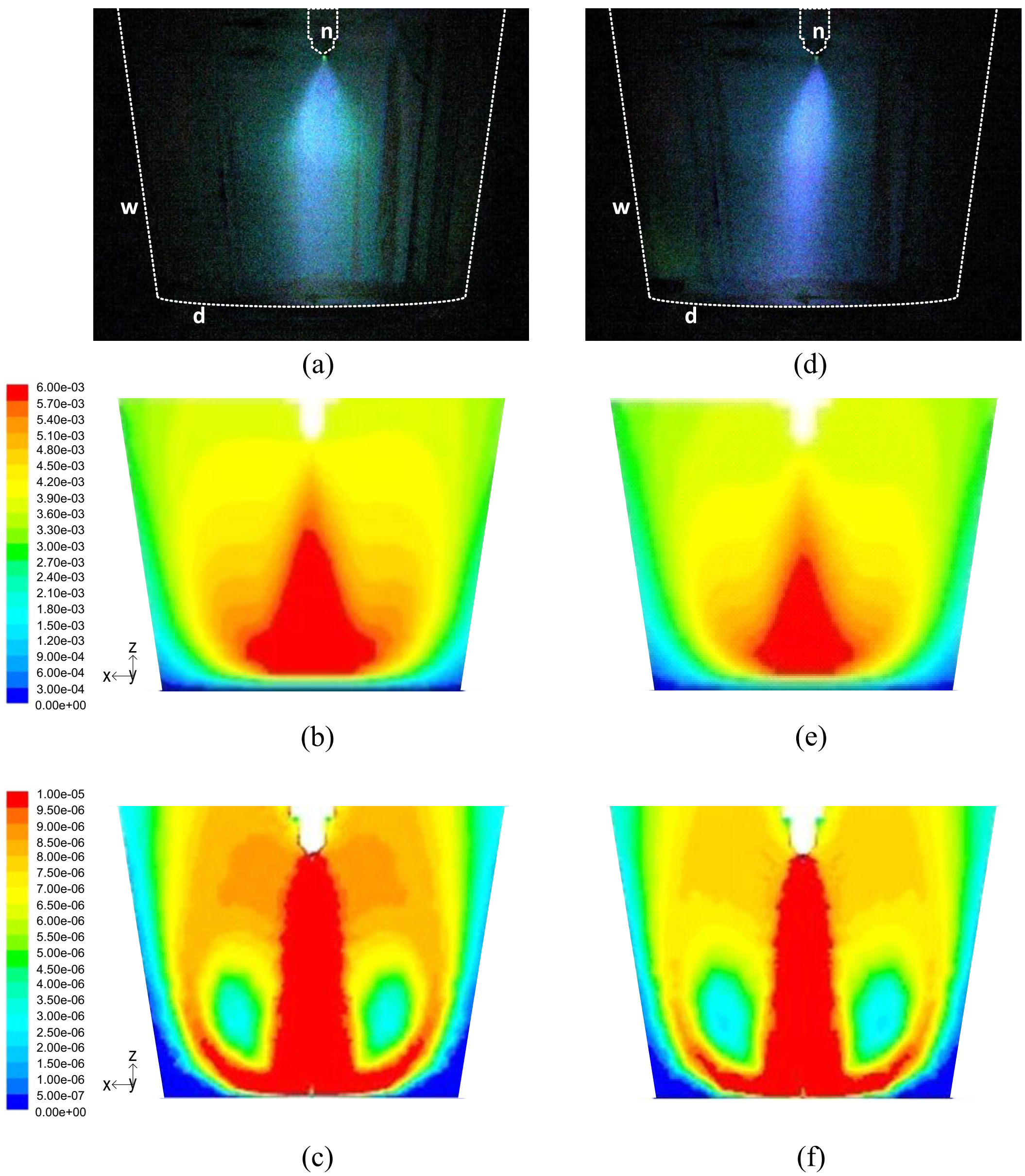

(a) (d)

(b) (e)

(c) (f)

Figure 10. Comparison between (a) contour of gas-solid-liquid DPM model-predicted time-averaged steady-state voidage, (b) gas-solid-liquid DPM model-predicted droplet tracks at t = 15s, (c) contour of gas-solid-liquid MFM-PBM model-predicted time-averaged steady-state voidage and (d) contour of gas-solid-liquid MFM-PBM model-predicted time-averaged steady-state liquid volume fraction.

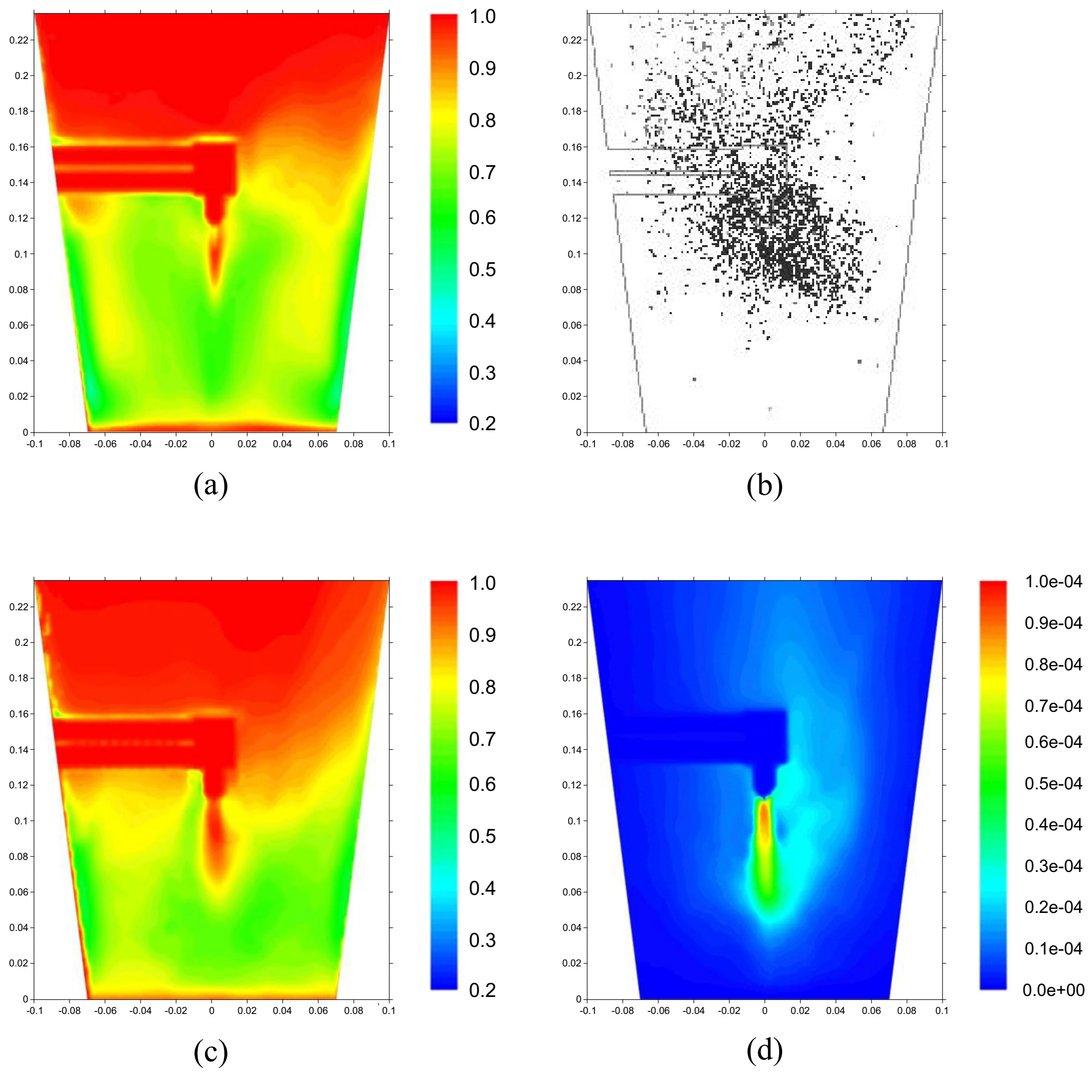

Table 1. Process variables used in this study ([a] indicates reference scenario).

Process variables	**Value**
Fluidisation air flow rate, $\dot{V}_f$ (m^3hr^{-1})	55, 76[a], 97
Atomisation air pressure, P_{at} (bar)	1.0, 2.0[a], 3.0
Liquid feed rate, $\dot{M}_l$ ($\times 10^{-4}$ kg s^{-1})	0.5, 1.0[a], 1.5

Table 2. Boundary conditions and simulation parameters.

Descriptor	**Value**
Primary phase (continuous)	Gas
Secondary phase (continuous)	Glass beads
Discrete phase	Water droplets
Solids particle size, d_s (µm)	196.54
Solids density, ρ_s (kg m^{-3})	2467
Solids loading, M_s (kg)	1
Gas phase density, ρ_g (kg m^{-3})	1.225
Liquid phase density, ρ_p (kg m^{-3})	998
Reactor bottom diameter (m)	0.15
Reactor top diameter (m)	0.30
Reactor height (m)	0.56

Highlights:

- Multiphase computational fluid dynamics model was built for fluidised bed coating
- Gas-solid fluidisation modeled in the Eulerian framework
- Two-fluid atomisation was described by discrete phase and population balance models
- Gas-liquid model-predicted spray pattern experimentally verified using UV illumination
- Population balance modelling proved viable alternative to discrete models